$FAPbBr_3$ Perovskite Quantum Dots as a Multifunctional Luminescent-Downshifting Passivation Layer for GaAs Solar Cells

Malek Rwaimi[a,1,*], Christopher G. Bailey[b,1], Peter J. Shaw[a], Thomas M. Mercier[a], Chirenjeevi Krishnan[a], Tasmiat Rahman[a], Pavlos G. Lagoudakis[b,c], Ray-Hua Horng[d], Stuart A. Boden[a], Martin D. B. Charlton[a]

[a] *Electronics & Computer Science, University of Southampton, Southampton, SO17 1BJ, United Kingdom.*
[b] *Physics and Astronomy, University of Southampton, Southampton, United Kingdom.*
[c] *Centre for Photonics and Quantum Materials, Skolkovo Institute of Science and Technology, Moscow 143026, Russia*
[d] *Institute of Electronics and Center for Emergent Functional Matter Science, National Yang Ming Chiao Tung University, Hsinchu 30010, Taiwan, ROC.*
[1] *These authors contributed equally*
** Corresponding Author. E-mail: mmer1u19@soton.ac.uk*

Abstract

Solar cells based on GaAs often include a wide-bandgap semiconductor as a window layer to improve surface passivation. Such devices often have poor photon-to-electron conversion efficiency at higher photon energies due to parasitic absorption. In this article, we deposit FAPbBr3 perovskite quantum dots on the AlInP window layer of a GaAs thin-film solar cell to improve the external quantum efficiency (EQE) across its entire absorption range, resulting in an 18% relative enhancement of the short-circuit current density. Luminescent downshifting from the quantum dots to the GaAs device contributes to a large effective enhancement of the internal quantum efficiency (IQE) at shorter wavelengths. Additionally, improved surface passivation of the window layer results in a 14-16% broadband increase of the IQE. These mechanisms combined with increased overall photon collection (antireflective effects) results in a doubling of the EQE in the ultraviolet region of the solar spectrum. Our results show a promising application of perovskite nanocrystals to improve the performance of well-established thin-film solar cell technologies.

Keywords: solar cells, quantum dots, perovskite, luminescence down shifting, gallium arsenide.

1 Introduction

Solar cells using III-V semiconductors have been extensively studied and engineered over the past few decades. Devices based on GaAs, with its favourable direct bandgap of 1.43 eV have demonstrated high power conversion efficiencies (PCEs) of 29.1% for thin-film crystal devices and 27.8% for single-crystal structures [1]. As the PCEs of devices approach the theoretical limit of ~33.5% [2], improving the match between the spectral response of the device and the solar spectrum provides a direct method to improve quantum efficiency. Many notable approaches to this have been explored, including plasmon resonance [3]–[5], multijunction solar cells [6]–[8], and photon upconversion [9], [10]. Another important route to achieve spectral matching is luminescence downshifting (LDS), where higher energy photons are collected in a material and re-emitted as lower energy photons to be collected in the charge-generating layer [11]. The LDS layer can be implemented via luminescent solar concentrators [12]–[14] or in general by ensuring it is optically coupled with the main absorbing layer [11], [15]–[17]. This process is particularly beneficial for devices

that demonstrate poor conversion efficiency of high-energy photons; for example, those that incorporate a wide-bandgap semiconductor as a window layer, in which charge carriers or excitons are generated but not efficiently extracted.

Material candidates for luminescent downshifting require a large absorption coefficient and high fluorescence efficiency to be beneficial for device performance. Suitable materials that have been successfully used include nanocrystals [15], [16], organic dyes [11], [15], [17] and rare-earth ion materials [18], [19]. Nanocrystals such as semiconductor quantum dots (QDs) have the unique property in that the bandgap can be modulated by changing the size of the QDs. With such versatility in their design and the compatibility with solution processing (colloidal QDs), these materials provide an inexpensive route for spectral matching via LDS [11], [20]–[22] and non-radiative energy transfer [20], [23]–[25]. Among the QD species considered for PV applications, perovskite nanocrystals are among the most interesting and have gained substantial attention in recent years [26]–[28]. These materials exhibit near-unity quantum yields [29], post-synthetically tuneable absorption and emission bands [29], and facile synthetic methodologies [30], [31].

Perovskite nanocrystals have so far been utilised as luminescent downshifting layers in only a small number of studies. For example, Meng and co-workers fabricated $MAPbBr_3$ QDs in polyacrylonitrile (PAN) and polyvinylidene fluoride (PVDF) composite films to improve the PCE of silicon solar cells by an absolute value of ~1% [32], [33]. In addition to this, Kim et al. used $CsPbBr_3$ nanocrystals as a LDS layer for a $Cu(In,Ga)Se_2$ (CIGS) solar cell, achieving a 4.5% relative improvement in the PCE [34].

We previously demonstrated the application of inorganic colloidal QDs as a resonance energy transfer- (RET) mediated LDS layer, resulting in a 14.6% relative increase in the photon conversion efficiency of an InGaP solar cell [24], and more recently an LDS/RET layer for interdigitated back contact silicon solar cells [20]. In this article, we use $FAPbBr_3$ perovskite QDs to significantly improve the quantum efficiency of a GaAs solar cell in the high photon-energy region of the solar spectrum via LDS. Improved surface passivation of the window layer combined with refractive index matching results in a further quantum-efficiency increase across the entire absorption range. We use optical and electrical characterisation methods to investigate the effect of the perovskite QD surface layer and provide insight to the mechanisms of the photocurrent enhancement.

2 Experimental Section

2.1. Fabrication of GaAs Device

The structure of GaAs solar cell was grown on 2-inch-diameter (100) GaAs wafers with a misorientation of 15° towards [111] using metalorganic chemical vapor deposition (MOCVD). Trimethylgallium (TMGa), and trimethylindium (TMIn) were used for the metal-organic precursors for group III-materials. Arsine (AsH_3) and phosphine (PH_3) were used as the precursors for group V-materials. After the epilayer growing, the AuBe/Au (50/150 nm) layers were deposited by e-beam evaporation system. These layers serve as both the *p*-contact layer and as the seed layer for electroplating of the Ni substrate. The GaAs substrate was then chemically etched to expose the GaInP etching stop layer. After the etching treatment, the device epilayer was transferred to a Ni substrate. Following this, a HCl: H_3PO_4 solution was applied for the removal GaInP etching stop layer. The AuGe/Au (50 nm/150 nm) was deposited on the *n*+ GaAs contact layer by E-beam evaporation as the front grid electrode. Finally, the $NH_4OH:H_2O_2:H_2O$ (1:9:40) was used to remove the n^+-GaAs contact layer.

2.2. Fabrication of FAPbBr3 Quantum Dots

Ethanol (100 mL, 99.8 % abs.) and oleylamine (OAm, 12.5 mL, 80-90 %) were mixed in a flask under intensive stirring before cooling in an ice water bath. Hydrobromic acid (HBr, 8.56 mL, 48 % in water) was then added and the flask placed under a continuous argon flow. The reaction was left to continue for 16 hours. The solution was then dried under vacuum and the resultant white powder was purified via multiple recrystallisation steps using diethyl ether as a solvent. The final powder was then dried in a vacuum oven at 80 °C for 16 hours.

A quantum dot solution of $FAPbBr_3$ was synthesized according to Protesescu *et al.* [28]. To achieve this, octadecene (ODE, 8 mL, 90 %) was added to a three-neck flask and dried under vacuum (< 10^{-4} mbar) for 1 hour at 120 °C. The flask was then flushed with argon, and lead acetate trihydrate (0.2 mmol, 0.076 g, 99.99 %), formamidinium acetate (0.75 mmol, 0.078 g), and oleic acid (OAc, 2 mL, 90 %) was added. This mixture was then dried under vacuum (< 10^{-4} mbar) for 30 minutes at 50 °C. The flask was flushed with argon and then placed under a steady flow of argon. After this, the temperature of the flask was raised to 130 °C and a solution containing as-synthesized oleylammonium bromide (OAmBr, 0.21 g, 0.6 mmol) dispersed in toluene (2 mL) was injected swiftly with a hot needle. The solution rapidly changed to an opaque chartreuse color.

The mixture was then placed immediately in an ice bath to quench the reaction. To purify the crude solution, toluene (10 mL) and acetonitrile (5 mL) was added and the mixture centrifuged for 10 minutes at 8500 rpm. The colourless, clear supernatant was then discarded, and the pellet dried and weighed. The pellet was finally dispersed in toluene to produce a solution of 80 mg/mL.

For the hybrid GaAs solar cell, the 80 mg/mL solution of $FAPbBr_3$ quantum dots was deposited on the surface of the AlInP window layer via spin coating at 3000 RPM. The thickness of this layer was determined to be approximately 100 nm from the results of the reflectance modelling discussed in the optical modelling section below.

2.3. Device Characterization

Measurements of the spectral responsivity and reflectance were performed using a commercial PV300 characterization system (Bentham). This allowed us to determine the external quantum efficiency (EQE) and internal quantum efficiency (IQE) by using data from a reference photodiode. During these measurements a monochromatic probe with a rectangular shape of approximately 3.3 mm^2 was incident onto the active area of the samples. During the scan, the photocurrent of the solar cell was measured across the wavelength range 300 – 1100 nm, with the device in the short-circuit configuration.

To measure specular and diffuse reflectance of the devices, the device was fixed at the back port of an integrating sphere and was irradiated at an incident angle of approximately 8°. The integrating sphere collects all the reflected light (specular and diffuse) to extract the total reflected light as a function of wavelength.

2.4. Characterization of FAPbBr3 Quantum Dots

UV-Vis absorbance data was obtained using a Shimadzu UV-2700 spectrophotometer. Fluorimetry data was measured using a Cary Eclipse Varian fluorescence spectrophotometer with an excitation wavelength of 350 nm. Transmission electron microscopy images were taken from a drop-cast sample of nanocrystals upon a copper-based grid. The acceleration voltage was set to 100 kV, and clear micrographs were obtainable from each sample.

2.5. Optical Modelling

The optical modelling was carried out using the freeware program OPAL 2 [35] to calculate the reflectance of the device with and without the layer of FAPbBr3 QDs. The devices were modelled with a reflective substrate followed by a structure of GaAs/GaInP/GaAs/AlInP for the reference device and GaAs/GaInP/GaAs/AlInP/FAPbBr3 QDs for the hybrid device. The refractive indices used for the GaAs, GaInP, and AlInP layers can be found in references [36], [37], [38], respectively. The optical constants of the FAPbBr3 QDs were determined by fitting the results from spectroscopic ellipsometry on a Silicon subtrate (J.A. Woolam M-2000).

---

3 Results and Discussion

3.1 $FAPbBr_3$ Perovskite Quantum Dots

For the hybrid GaAs solar cell, we fabricated $FAPbBr_3$ nanocrystals as described in the experimental section. The purified $FAPbBr_3$ nanocrystal solution was subjected to UV-Vis absorbance, fluorimetry, and transmission electron microscopy (TEM) analysis, shown in Figure 1.

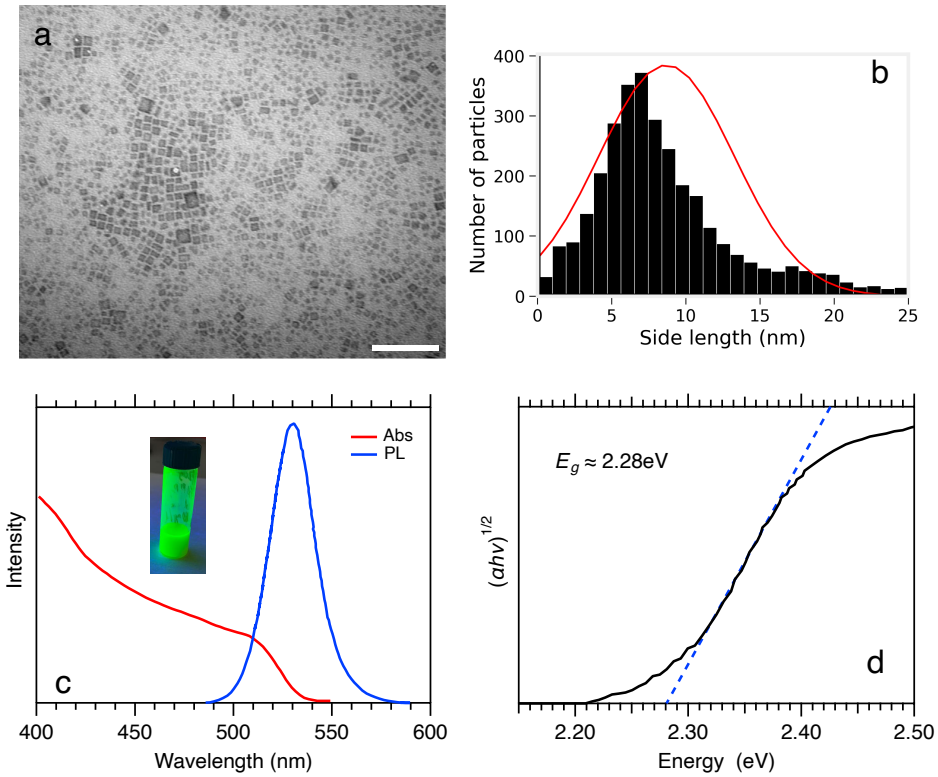

Fig 1. a) A transmission electron microscope (TEM) image of the $FAPbBr_3$ nanocrystals. Scale bar 100 nm. b) The distribution of the side lengths of the nanocrystals. The red line shows a normal distribution with a mean and standard deviation of the nanocrystal sizes. c) The absorbance (red) and emission (blue) spectrum of the FAPbBr3 nanocrystal solution. d) Tauc plot for the nanocrystal solution. The blue dotted line shows a linear fit to the fundamental absorption. An estimate for the bandgap is found by the intersection of the fit and the x-axis.

The electron micrograph (Figure 1a) shows the ensemble of cubic particles with edge lengths on the order of 10 nm. Figure 1b shows the distribution of nanocrystal sizes, with a mean edge length of 8.71 nm and a standard deviation of 4.57 nm. The obtained solution has an optical profile typical of quantum-dot solutions (Fig. 1c): a single emission at 530 nm with a narrow full-width half-maximum of 26 nm, and an absorption onset at approximately 540 nm. We carried out a modified Tauc-plot analysis, shown in Figure 1d. The intersection of the linear fit of the fundamental absorption and the x-axis is used as an approximation of the average bandgap energy of the nanocrystals. This analysis yields a bandgap energy of $E_g = 2.28$ eV. We previously characterized the stability of the nanocrystals in ambient conditions, showing their capability to withstand high intensity light exposure over several days while maintaining significant luminescence [39].

3.2 Hybrid GaAs Solar Cell

The epitaxial structure of the reference GaAs solar cell is shown in Figure 2a. We deposited the $FAPbBr_3$ perovskite QDs onto the window layer of the GaAs cell by spin coating as described in the experimental section to form a thin film approximately 100 nm thick. We determined the spectral performance of this device by measuring the external quantum efficiency (EQE) before and after depositing the QD layer, shown in Figure 2b.

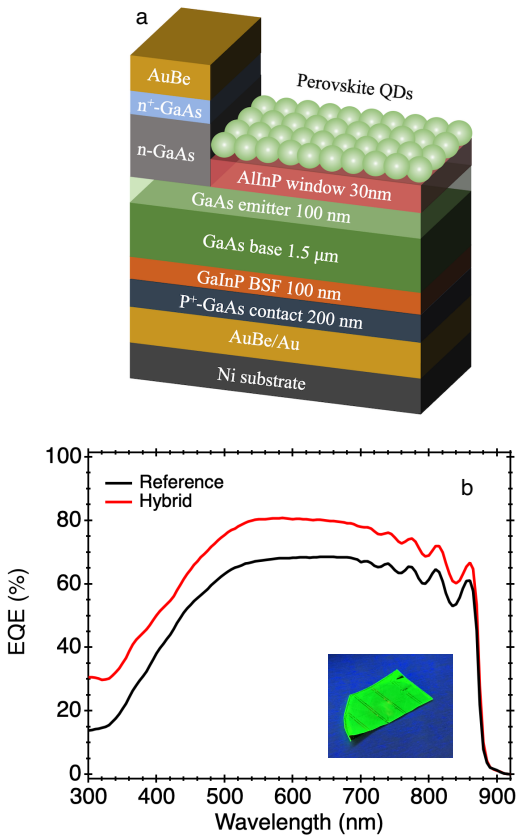

Fig 2. a) Schematic of the hybrid GaAs solar cell. The perovskite QDs are deposited on the window layer via spin coating. b) EQE spectra for the reference and hybrid GaAs solar cell.

We observed an enhancement of the EQE across the entire absorption range of the GaAs solar cell after depositing the $FAPbBr_3$ QDs, as shown in Figure 2b. The short-circuit current density can be calculated from the EQE response using the equation:

$$J_{SC} = q\int_{\lambda_1}^{\lambda_2} \mathrm{EQE}(\lambda)\Phi(\lambda)d\lambda\,, \tag{1}$$

where $\Phi(\lambda)$ is the photon flux in the AM1.5G solar spectrum. Following the hybridization, the device exhibited a higher short-circuit current density (*J*sc) of 23.24 mA/cm^2 compared to the reference cell with a *J*sc of 19.74 mA/cm^2, corresponding to a relative enhancement of 17.7%. We associate this observation to three main mechanisms resulting from the addition of the quantum dot layer: 1) luminescent down shifting (LDS) from the QDs to the GaAs, 2) an anti-reflection (AR) effect due to increased scattering and refractive index matching, and 3) improved passivation of the device, reducing surface recombination. We also investigated the spatial uniformity of the EQE across the area of the device by sampling different locations, using a beam with a size of <5% of the total sample area (see methods). The corresponding data is shown in the supporting information (Figure S1). The reference device exhibited a maximum of ~15% relative variation in EQE at shorter wavelengths and ~5% at 600 nm. The relative variation in EQE was increased to ~18% at shorter wavelengths and reduced slightly to ~4% at 600 nm following the deposition of the QDs, suggesting high uniformity of the surface coverage of the QDs.

To investigate the optical properties of the device further, we measured the reflectance spectra of the GaAs device before and after depositing the quantum dots, shown in Figure 3a.

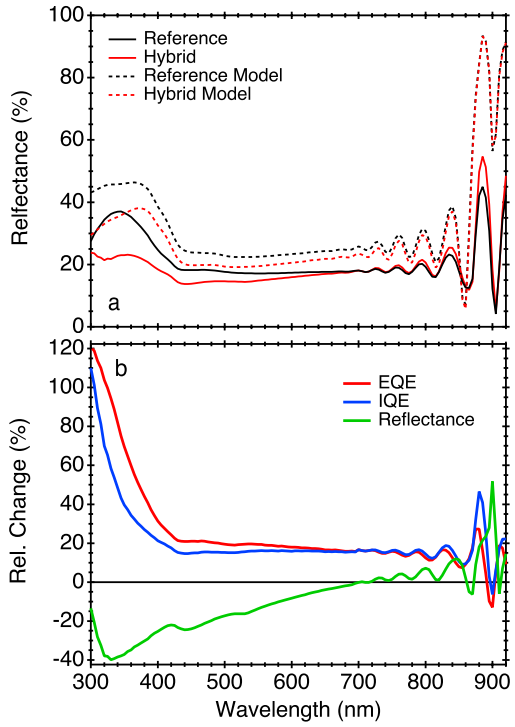

Fig 3. a) Reflectance spectra for the reference and hybrid GaAs solar cell along with the modelled data (dashed curves). b) Relative change in EQE, IQE and reflectance spectra after hybridization expressed as a percentage versus wavelength.

The measurement shows a decrease of reflectance at the wavelength range below ~ 700 nm due to the addition of the QD layer providing better refractive index matching and absorbing light at photon energies above its bandgap. This is in good agreement with results from optical modelling (see Experiment section for details) shown in Figure 3a which suggest an expected decrease in the reflectance in the same spectral range. The measured reduction in reflectance is significantly greater than that predicted by using the model at shorter wavelengths, which can be explained by two reasons: the first is the optical constants for the perovskite QDs were obtained by fitting the results of ellipsometry measurements on a Silicon substrate and therefore may have slightly different morphology and optical features. The second reason is that the model does not account for the texturing introduced by the QD layer, which is likely to further reduce the reflectance due to scattering from agglomerates of QDs.

Using the results from the reflectance and EQE measurements, we were able to determine the internal quantum efficiency (IQE) using the relationship:

$$\mathrm{IQE}(\lambda) = \frac{\mathrm{EQE}(\lambda)}{1 - R(\lambda) - T(\lambda)}, \tag{2}$$

where $R(\lambda)$ is the reflectance and $T(\lambda)$ is the transmittance of the sample. The transmittance was assumed to be zero since the GaAs solar cell had a highly reflective back contact.

The relative change in IQE was calculated using the equation:

$$\mathrm{IQE}_{\mathrm{rel}}(\lambda) = \frac{\mathrm{IQE}_{\mathrm{hyb}}(\lambda) - \mathrm{IQE}_{\mathrm{ref}}(\lambda)}{\mathrm{IQE}_{\mathrm{ref}}(\lambda)}, \tag{3}$$

where the subscripts hyb and ref refer to the hybrid and reference samples, respectively. Similar analysis was performed for the reflectance and EQE spectra, and the results are shown in Figure 3b to highlight the regions of the spectrum which are enhanced.

On observation of the relative IQE (Figure 3b), an almost constant enhancement of ~ 14.5-15.5% is achieved across all wavelengths above 425 nm. At shorter wavelengths, a much larger enhancement of the IQE is observed which rises with decreasing wavelength and can be attributed to LDS. The shape of the relative IQE enhancement follows the

absorption spectrum of the perovskite QDs at the optical transition observed at ~425 nm (Figure 1). For the reference device, the reflectance increases sharply below ~425 nm; a feature which is far less pronounced in the hybrid device, contributing the shape of the relative EQE enhancement. However, the relative EQE enhancement does not correspond exactly to the shape of the relative change in the reflectance (Figure 3b), suggesting LDS is the dominant mechanism for the EQE enhancement at shorter wavelengths. We did not observe a correlation between the relative IQE and the onset of the absorption of the QDs at ~540 nm, partly due to the absorption of the QDs being lower at this longer-wavelength region.

The EQE enhancement at long wavelengths outside the absorption range of the quantum dots is partially owed to the improved refractive index matching in the hybrid device but also to another contributing factor, indicated by the increase in the IQE across this wavelength range. We associate this IQE enhancement with improved passivation of the surface of the device following deposition of the QDs, since this effect will be irrespective of photon energy [40]. Results from a previous study using QDs of a different composition, with the same ligand (oleic acid) as a LDS layer for InGaP solar cells did not allude to any passivation effects [24]. Since in this current study both the window layer and the ligand of the QD are the same material as those used previously, we propose that the effect is not due to a chemical passivation but instead a field-effect passivation [41]–[43]. Field-effect passivation can occur when a dielectric layer forms a dipole, and the resultant field causes a spatial change in surface carrier concentrations. A reduction in the relative proportion of majority carriers (electrons in the emitter layer) versus minority carriers would reduce the surface recombination velocity by reducing diffusion of minority carriers towards the surface [44], [45]. Further studies are required to investigate the potential field-effect passivation provided by perovskite QDs.

The change in IQE after the addition of the LDS layer can be attributed to two main components:

$$\Delta\mathrm{IQE}(\lambda) = \Delta\mathrm{IQE}_{\mathrm{optical}}(\lambda) + \Delta\mathrm{IQE}_{\mathrm{pass}}, \tag{4}$$

where $\Delta\mathrm{IQE}_{\mathrm{optical}}(\lambda)$ is the wavelength-dependent enhancement provided by the LDS layer and $\Delta\mathrm{IQE}_{\mathrm{pass}}$ is the increase due to improved passivation, which we approximate to be wavelength-independent. For the addition of a regular LDS layer (without enhancement from RET), the IQE of the hybrid device can be expressed as:

$$\mathrm{IQE}_{\mathrm{hyb}}(\lambda) = \mathrm{IQE}_{\mathrm{ref}}(\lambda)\left(1 - A_{QD}(\lambda)\right) + \eta_{LDS}(\lambda)\mathrm{IQE}_{\mathrm{ref}}\left(\lambda_{QD}\right) + \Delta\mathrm{IQE}_{\mathrm{pass}}, \tag{4}$$

where $A_{QD}(\lambda)$ is the absorption spectrum of the QDs, $\mathrm{IQE}_{\mathrm{ref}}\left(\lambda_{QD}\right)$ is the IQE of the reference device at the emission wavelength of the QDs, and $\eta_{LDS}(\lambda)$ is the efficiency of the LDS, given by the product of the QD absorption, $A_{QD}(\lambda)$, and the photoluminescence quantum yield (PLQY) of the QDs. We calculated the upper limit of the IQE spectrum for the hybrid device without the RET enhancement by assuming a PLQY of 100%, which is presented in Figure 4. We obtained the absorption spectrum of the 100 nm QD layer using the extinction coefficient from ellipsometry results. We approximate the IQE increase due to improved passivation by using the average relative increase at photon energies below the bandgap of the QDs, which is found to be 15.8% (Figure 3b).

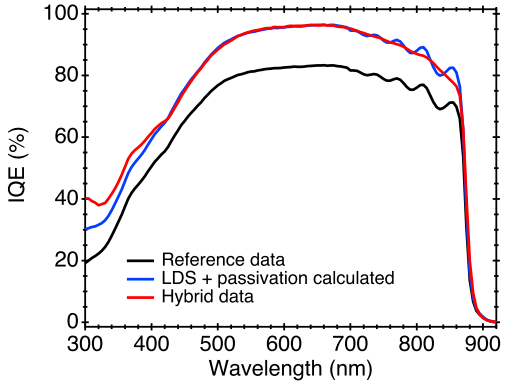

Fig 4. Measured IQE spectra of the reference and hybrid devices. The blue spectrum shows the calculated IQE for the reference device with a regular 100 nm LDS layer of $FAPbBr_3$ QDs with a PLQY of 100%.

As can be seen in Figure 4, there is a clear discrepancy between the measured IQE spectrum of the hybrid device, and the spectrum calculated for a regular $FAPbBr_3$ QD LDS layer with a PLQY of 100%. This provides evidence to suggest that there is an additional contribution to the IQE enhancement. It was previously shown that carriers generated in the AlInP layer can undergo non-radiative resonance energy transfer (RET), generating excitons in a layer of QDs deposited on the window layer, reducing the effect of parasitic absorption [24]. We propose the difference between the measured and expected IQE enhancement in our study is accounted for by the same RET mechanism. Figure 5 illustrates the proposed LDS mechanisms for the photocurrent enhancement observed in the hybrid device.

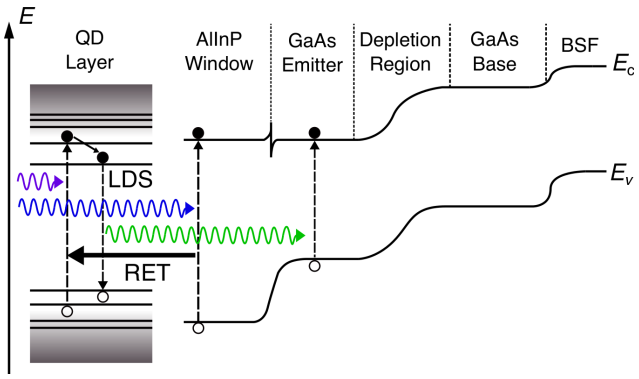

Fig 5. Proposed mechanisms for the photocurrent enhancement in the hybrid GaAs solar cell. The perovskite QD layer absorbs higher energy photons and re-emits lower energy photons which are absorbed in the GaAs emitter layer. Additionally, photons absorbed in the window layer are non-radiatively transferred to the QD layer via RET, further increasing the supply of photons to undergo LDS in the QD layer.

The bandgap of the AlInP window layer is 2.275 eV (546 nm) [46] which is very close to the absorption onset of the QDs (Figure 1). This large spectral overlap, combined with the indirect nature of the AlInP bandgap permits a high probability for non-radiative energy transfer from the AlInP window layer to the QD layer, which increases the supply of photons in the QD layer to undergo LDS.

4 Conclusion

In conclusion, we have shown that perovskite quantum dots can be utilized as a multifunctional surface layer for high-efficiency GaAs solar cells to increase the overall photocurrent. Luminescent downshifting occurs from the QDs to the GaAs device which is likely being supplied partially by photogenerated species undergoing RET from the AlInP window layer to the QDs. The QD layer also provides increased scattering, improved refractive index matching, and a field-effect passivation which reduces surface recombination. The hybridization leads to an ~18% relative enhancement of the photocurrent and a 50-120% relative increase of the EQE in the ultraviolet wavelength range. Future studies should focus on exploring quantum dots of different perovskite compositions and fundamental investigations to fully understand the photocurrent enhancement mechanisms.

Declaration of Interest

The authors declare that they have no known competing financial interests or personal relationships that could have appeared to influence the work reported in this paper.

Acknowledgment

T. Rahman and S.A. Boden acknowledge support from the Supersolar Solar Energy Hub (EPSRC grants EP/J017361/1 and EP/M014797/1). P. Shaw and M.D.B Charlton acknowledge funding by the EPSRC (EP/M508147/1). C. Bailey and P. Lagoudakis acknowledge funding from the EPRSC (grant EP/L01551X/1).

References

[1] NREL, "NREL Efficiency Chart," 2019. [Online]. Available: https://www.nrel.gov/pv/cell-efficiency.html. [Accessed: 06-Jan-2020].

[2] O. D. Miller, E. Yablonovitch, and S. R. Kurtz, "Strong internal and external luminescence as solar cells approach the Shockley-Queisser limit," *IEEE J. Photovoltaics*, vol. 2, no. 3, pp. 303–311, 2012.

[3] J. Yang *et al.*, "Plasmonic polymer tandem solar cell," *ACS Nano*, vol. 5, no. 8, pp. 6210–6217, 2011.

[4] A. Polman, "Plasmonic Solar Cells," *Opt. Express*, vol. 16, no. 26, pp. 21793–21800, 2018.

[5] X. Wang *et al.*, "Self-Constructed Multiple Plasmonic Hotspots on an Individual Fractal to Amplify Broadband Hot Electron Generation," *ACS Nano*, vol. 15, no. 6, pp. 10553–10564, 2021.

[6] J. Werner *et al.*, "Efficient Monolithic Perovskite/Silicon Tandem Solar Cell with Cell Area >1 cm2," *J. Phys. Chem. Lett.*, vol. 7, no. 1, pp. 161–166, 2016.

[7] J. You *et al.*, "A polymer tandem solar cell with 10.6% power conversion efficiency," *Nat. Commun.*, vol. 4, 2013.

[8] R. R. King *et al.*, "40% efficient metamorphic GaInPGaInAsGe multijunction solar cells," *Appl. Phys. Lett.*, vol. 90, no. 18, pp. 90–93, 2007.

[9] A. Shalav, B. S. Richards, and M. A. Green, "Luminescent layers for enhanced silicon solar cell performance: Up-conversion," *Sol. Energy Mater. Sol. Cells*, vol. 91, no. 9, pp. 829–842, 2007.

[10] T. Trupke, M. A. Green, and P. Würfel, "Improving solar cell efficiencies by up-conversion of sub-band-gap light," *J. Appl. Phys.*, vol. 92, no. 7, pp. 4117–4122, 2002.

[11] E. Klampaftis, D. Ross, K. R. McIntosh, and B. S. Richards, "Enhancing the performance of solar cells via luminescent down-shifting of the incident spectrum: A review," *Solar Energy Materials and Solar Cells*, vol. 93, no. 8. North-Holland, pp. 1182–1194, 01-Aug-2009.

[12] M. G. Debije and P. P. C. Verbunt, "Thirty years of luminescent solar concentrator research: Solar energy for the built environment," *Adv. Energy Mater.*, vol. 2, no. 1, pp. 12–35, 2012.

[13] H. Zhao, R. Sun, Z. Wang, K. Fu, X. Hu, and Y. Zhang, "Zero-Dimensional Perovskite Nanocrystals for Efficient Luminescent Solar Concentrators," *Adv. Funct. Mater.*, vol. 29, no. 30, pp. 1–8, 2019.

[14] H. Zhao *et al.*, "Efficient and stable tandem luminescent solar concentrators based on carbon dots and perovskite quantum dots," *Nano Energy*, vol. 50, no. May, pp. 756–765, 2018.

[15] W. G. J. H. M. Van Sark, A. Meijerink, R. E. I. Schropp, J. A. M. Van Roosmalen, and E. H. Lysen, "Enhancing solar cell efficiency by using spectral converters," in *Solar Energy Materials and Solar Cells*, 2005, vol. 87, no. 1–4, pp. 395–409.

[16] V. Švrček, A. Slaoui, and J. C. Muller, "Silicon nanocrystals as light converter for solar cells," in *Thin Solid Films*, 2004, vol. 451–452, pp. 384–388.

[17] B. S. Richards and K. R. McIntosh, "Overcoming the poor short wavelength spectral response of CdS/CdTe photovoltaic modules via luminescence down-shifting: Ray-tracing simulations," *Prog. Photovoltaics Res. Appl.*, vol. 15, no. 1, pp. 27–34, Jan. 2007.

[18] T. Jin, S. Inoue, S. Tsutsumi, K. I. Machida, and G. Y. Adachi, "High conversion efficiency photovoltaic cell enhanced by lanthanide complex phosphor film coating," *Chem. Lett.*, no. 2, pp. 171–172, May 1997.

[19] S. Marchionna *et al.*, "Photovoltaic quantum efficiency enhancement by light harvesting of organo-lanthanide complexes," *J. Lumin.*, vol. 118, no. 2, pp. 325–329, Jun. 2006.

[20] C. Krishnan *et al.*, "Efficient light harvesting in hybrid quantum dot-interdigitated back contact solar cells via resonant energy transfer and luminescent downshifting," *Nanoscale*, vol. 11, no. 40, pp. 18837–18844, Oct. 2019.

[21] D. Alonso-Álvarez *et al.*, "Luminescent down-shifting experiment and modelling with multiple photovoltaic technologies," *Prog. Photovoltaics Res. Appl.*, vol. 23, no. 4, pp. 479–497, Apr. 2015.

[22] X. Huang, S. Han, W. Huang, and X. Liu, "Enhancing solar cell efficiency: The search for luminescent materials as spectral converters," *Chem. Soc. Rev.*, vol. 42, no. 1, pp. 173–201, Dec. 2013.

[23] S. Chanyawadee, R. T. Harley, M. Henini, D. V. Talapin, and P. G. Lagoudakis, "Photocurrent enhancement in hybrid nanocrystal quantum-dot p-i-n photovoltaic devices," *Phys. Rev. Lett.*, vol. 102, no. 7, p. 077402, Feb. 2009.

[24] M. Brossard *et al.*, "Novel non-radiative exciton harvesting scheme yields a 15% efficiency improvement in high-efficiency III-V solar cells," *Adv. Opt. Mater.*, vol. 3, no. 2, pp. 263–269, 2015.

[25] P. J. Shaw *et al.*, "Resonant energy transfer properties of perovskite nanocrystals," in *Proc.SPIE*, 2020, vol. 11291.
[26] A. Kojima, K. Teshima, Y. Shirai, and T. Miyasaka, "Organometal halide perovskites as visible-light sensitizers for photovoltaic cells," *J. Am. Chem. Soc.*, vol. 131, no. 17, pp. 6050–6051, 2009.
[27] L. Protesescu *et al.*, "Nanocrystals of Cesium Lead Halide Perovskites (CsPbX3, X = Cl, Br, and I): Novel Optoelectronic Materials Showing Bright Emission with Wide Color Gamut," *Nano Lett.*, vol. 15, no. 6, pp. 3692–3696, 2015.
[28] L. Protesescu *et al.*, "Monodisperse Formamidinium Lead Bromide Nanocrystals with Bright and Stable Green Photoluminescence," *J. Am. Chem. Soc.*, vol. 138, no. 43, pp. 14202–14205, 2016.
[29] J. De Roo *et al.*, "Highly Dynamic Ligand Binding and Light Absorption Coefficient of Cesium Lead Bromide Perovskite Nanocrystals," *ACS Nano*, vol. 10, no. 2, pp. 2071–2081, 2016.
[30] I. Levchuk *et al.*, "Ligand-assisted thickness tailoring of highly luminescent colloidal CH3NH3PbX3 (X = Br and I) perovskite nanoplatelets," *Chem. Commun.*, vol. 53, no. 1, pp. 244–247, 2017.
[31] I. Levchuk *et al.*, "Brightly Luminescent and Color-Tunable Formamidinium Lead Halide Perovskite FAPbX3 (X = Cl, Br, I) Colloidal Nanocrystals," *Nano Lett.*, vol. 17, no. 5, pp. 2765–2770, 2017.
[32] L. Meng, L. Shi, Y. Ge, J. Tang, Y. Chen, and H. Zhong, "Photon management of combining nanostructural antireflection and perovskite down-shifting composite films for improving the efficiency of silicon solar cells," *Sol. Energy Mater. Sol. Cells*, vol. 220, p. 110856, Jan. 2021.
[33] L. Meng *et al.*, "Improving the efficiency of silicon solar cells using in situ fabricated perovskite quantum dots as luminescence downshifting materials," *Nanophotonics*, vol. 9, no. 1, pp. 93–100, Jan. 2020.
[34] Y. C. Kim *et al.*, "Luminescent down-shifting CsPbBr3 perovskite nanocrystals for flexible Cu(In,Ga)Se2 solar cells," *Nanoscale*, vol. 12, no. 2, pp. 558–562, 2020.
[35] K. R. McIntosh and S. C. Baker-Finch, "OPAL 2: Rapid optical simulation of silicon solar cells," *Conf. Rec. IEEE Photovolt. Spec. Conf.*, pp. 265–271, 2012.
[36] D. E. Aspnes and A. A. Studna, "Dielectric functions and optical parameters of Si, Ge, GaP, GaAs, GaSb, InP, InAs, and InSb from 1.5 to 6.0 eV," *Phys. Rev. B*, vol. 27, no. 2, pp. 985–1009, Jan. 1983.
[37] M. Schubert, V. Gottschalch, C. M. Herzinger, H. Yao, P. G. Snyder, and J. A. Woollam, "Optical constants of Ga x In 1−x P lattice matched to GaAs," *J. Appl. Phys.*, vol. 77, p. 3416, 1995.
[38] E. Ochoa-Martínez *et al.*, "Refractive indexes and extinction coefficients of n- and p-type doped GaInP, AlInP and AlGaInP for multijunction solar cells," *Sol. Energy Mater. Sol. Cells*, vol. 174, no. September 2017, pp. 388–396, 2018.
[39] P. Shaw, T. M. Mercier, C. Bailey, A. G. Kanaras, P. G. Lagoudakis, and M. D. B. Charlton, "High intensity photodegradation of lead halide perovskite nanocrystals," in *Light-Emitting Devices, Materials, and Applications XXIV*, 2020, vol. 11302, no. February 2020, p. 1130208.
[40] F. Sgrignuoli *et al.*, "Purcell effect and luminescent downshifting in silicon nanocrystals coated back-contact solar cells," *Sol. Energy Mater. Sol. Cells*, vol. 132, pp. 267–274, 2015.
[41] S. W. Glunz, D. Biro, S. Rein, and W. Warta, "Field-effect passivation of the SiO2-Si interface," *J. Appl. Phys.*, vol. 86, no. 1, pp. 683–691, Jun. 1999.
[42] G. Dingemans, N. M. Terlinden, D. Pierreux, H. B. Profijt, M. C. M. Van De Sanden, and W. M. M. Kessels, "Influence of the oxidant on the chemical and field-effect passivation of Si by ALD Al2 O3," *Electrochem. Solid-State Lett.*, vol. 14, no. 1, p. H1, Oct. 2011.
[43] F. Wang *et al.*, "Interface Dipole Induced Field-Effect Passivation for Achieving 21.7% Efficiency and Stable Perovskite Solar Cells," *Adv. Funct. Mater.*, vol. 31, no. 5, p. 2008052, Jan. 2021.
[44] R. S. Bonilla, B. Hoex, P. Hamer, and P. R. Wilshaw, "Dielectric surface passivation for silicon solar cells: A review," *Phys. Status Solidi Appl. Mater. Sci.*, vol. 214, no. 7, p. 1700293, Jul. 2017.
[45] A. Cuevas and D. Yan, "Misconceptions and misnomers in solar cells," *IEEE J. Photovoltaics*, vol. 3, no. 2, pp. 916–923, 2013.
[46] X. Yan *et al.*, "Enhanced omnidirectional photovoltaic performance of solar cells using multiple-discrete-layer tailored- and low-refractive index anti-reflection coatings," *Adv. Funct. Mater.*, vol. 23, no. 5, pp. 583–590, 2013.